ACS APPLIED MATERIALS & INTERFACES

www.acsami.org

Research Article

Construction of Bio-Nano Interfaces on Nanozymes for Bioanalysis

Jie Li, Na Lu,* Suping Han, Xuemei Li, Mengqin Wang, Mengchao Cai, Zisheng Tang,* and Min Zhang*

Cite This: *ACS Appl. Mater. Interfaces* 2021, 13, 21040−21050

Read Online

ACCESS | Metrics & More | Article Recommendations | Supporting Information

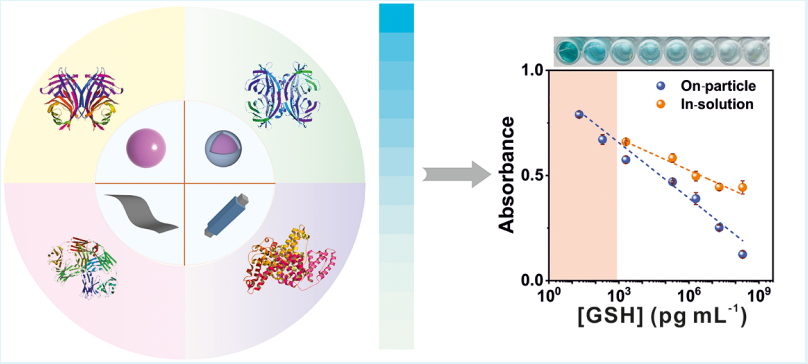

ABSTRACT: Nanomaterials with enzyme-like activity (nanozymes) have been of great interest in broad applications ranging from biosensing to biomedical applications. Despite that much effort has been devoted to the development of the synthesis and applications of nanozymes, it is essential to understand the interactions between nanozymes and most commonly used biomolecules, i.e., avidin, streptavidin (SA), bovine serum albumin (BSA), immunoglobulin G (IgG), and glutathione (GSH), yet they have been rarely explored. Here, a series of bio-nano interfaces were constructed through direct immobilization of proteins on a variety of iron oxide and carbon-based nanozymes with different dimensions, including Fe_3O_4 nanoparticles (NPs, 0D), Fe_3O_4@C NPs (0D), Fe_3O_4@C nanowires (NWs, 1D), and graphene oxide nanosheets (GO NSs, 2D). Such interfaces enabled the modulation of the catalytic activities of the nanozymes with varying degrees, which allowed a good identification of multiplex proteins with high accuracy. Given the maximum inhibition on Fe_3O_4@C NP by BSA, we established molecular switches based on aptamer and toehold DNA, as well as Boolean logic gates (AND and NOR) in response to both DNA and proteins. Also importantly, we developed an on-particle reaction strategy for colorimetric detection of GSH with ultrahigh sensitivity and good specificity. The proposed sensor achieved a broad dynamic range spanning 7 orders of magnitude with a detection limit down to 200 pg mL^{-1}, which was better than that of an in-solution reaction-based biosensor by 2 orders of magnitude. Furthermore, we explored the mechanisms of the interactions at bio-nano interfaces by studying the interfacial factors, including surface coverage, salt concentration, and the curvature of the nanozyme. This study offered new opportunities in the elaborate design and better utilization of nanozymes for bioanalysis in clinical diagnosis and in vivo detection.

KEYWORDS: *nanozymes, peroxidase-like, bio-nano interface, protein, logic gate, GSH detection*

INTRODUCTION

With the significant progress in nanoscience and nanotechnology, nanostructured materials have attracted increasing attention in the application of biosensing,[1−7] bioimaging,[8−13] energy storage,[14−16] absorption,[17−19] and catalysis.[20−25] Among them, nanomaterials with enzyme-like activity (nanozymes),[26,27] have emerged as potential replacements for natural enzymes due to their good stability, easy synthesis, and biocompatibility. So far, a plethora of nanozymes, including iron oxide,[28−30] noble metal,[31,32] carbon,[33,34] and metal organic frameworks (MOF)-based nanomaterials,[35−37] have been designed and synthesized via wet chemical method, templating method, and so on. Taking advantage of the intrinsic enzyme-mimicking characteristic, nanozymes have been extensively used for biomedical applications from disease diagnosis[38−41] to cancer therapy.[42,43] Despite that a growing number of studies have been performed over the past two decades, a fundamental investigation to understand the nano-bio interactions[44] between biomolecules and nanozymes needs to be fully addressed, which thus in turn provides new

Received: March 8, 2021
Accepted: April 21, 2021
Published: April 29, 2021

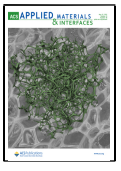

https://doi.org/10.1021/acsami.1c04241
ACS Appl. Mater. Interfaces 2021, 13, 21040−21050

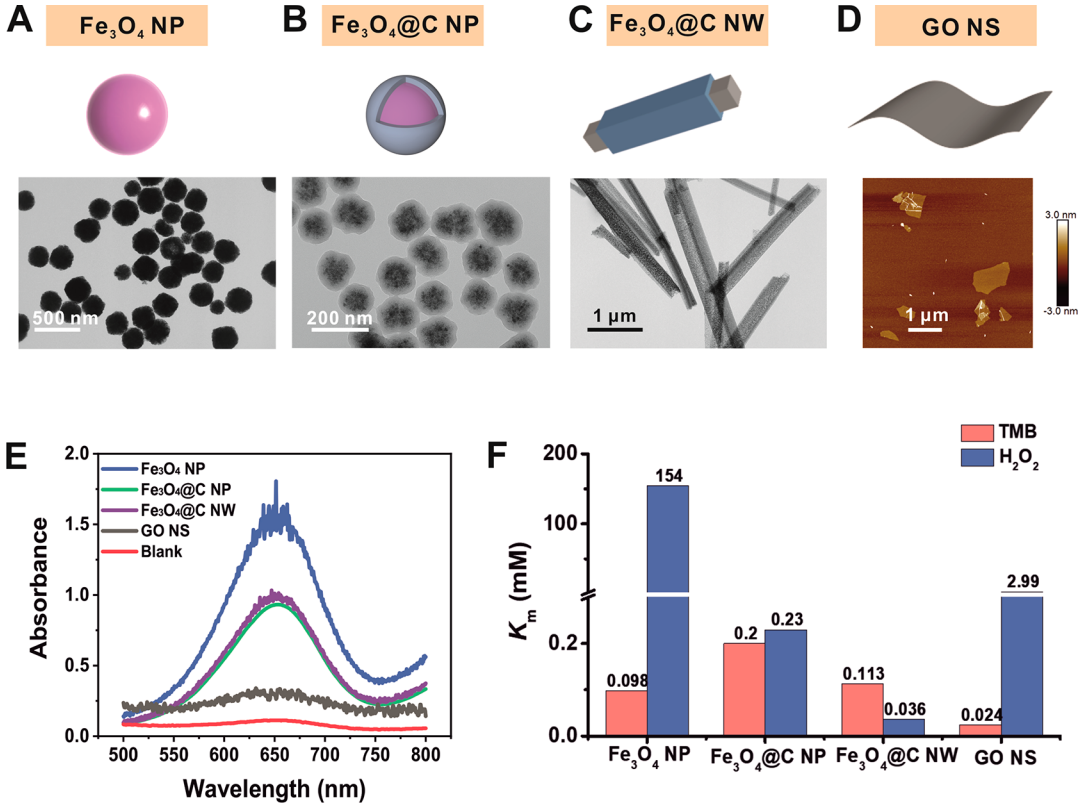

Figure 1. Characterization and catalytic performance of nanozymes. (A–D) Schematic illustrations and TEM images of Fe_3O_4 NP, Fe_3O_4@C NP, Fe_3O_4@C NW, and AFM image of GO NS. (E) UV–vis spectra of TMB solutions catalyzed by different nanomaterials. (F) The K_m values of different nanomaterials to the substrates from Michaelis–Menten kinetics. The catalytic reaction was carried out by using 20 μg mL^{-1} nanozyme in 0.2 M HAc-NaAc buffer (pH 4.0) containing 1 mM TMB and 5 mM H_2O_2.

opportunities for rationalizing design and utilization of nanozymes.

To overcome this challenge, some recent studies of DNA-functionalized nanozymes have been reported.[45,46] When DNA meets nanostructured systems, physicochemical forces, thermodynamics, and kinetics form bio-nano interfaces with altered catalytic properties. For example, single-strand DNA (ssDNA) engineering nanointerfaces could enhance the peroxidase-like properties of Fe_3O_4 nanoparticles (NPs) toward 3,3',5,5'-tetramethylbenzidine (TMB) oxidation.[47] Additionally, a fine-tuning of the catalytic activity of Fe_3O_4 NPs had been achieved by modification of different structured DNA ligands on the inorganic surface.[48] Besides DNA, small biomolecules, such as avidin, streptavidin (SA), bovine serum albumin (BSA), angiten, and peptide, are other most commonly used biomaterials in biomedical applications, which not only provide molecular recognition to target biomolecules (e. g., immunosorbent assays) but also are suitable for further cross-linking with other active biomolecules for specific affinity (e.g., affinity coupling, blocking agent).[49] However, compared to the mainstream researches of studying the influence of DNA functionalization, a parallel significant role of the functionalization of small molecule on nanozymes still remains unclear, and their application in biological detection has scarcely been explored so far.

Herein, we rationally design and construct a series of bio-nano interfaces by modifying avidin, SA, BSA, and immunoglobulin G (IgG) on the inorganic surface of nanozymes. Such interfaces enable inhibited peroxidase-like activities of the nanozymes with varying degrees. Moreover, we build Boolean logic gates (AND and NOR) utilizing the intelligent bio-nano interfaces, which are capable of response simultaneously toward DNA and proteins. By virtue of the unique feature, we also successfully develop a novel sensing manner with the on-particle reaction for the detection of glutathione (GSH), which exhibits better analytical performance than that of the in-solution reaction. Moreover, we in-depth analyzed the inhibited mechanisms of the interactions at bio-nano interfaces by studying the interfacial factors, such as surface coverage, salt concentration, and curvature. Taken together, as the biorecognition element combines with the bio-nano interface, the biohybrid nanomaterial can be readily utilized for downstream applications ranging from biosensing to biomolecule computing.

RESULTS AND DISCUSSION

Characterization and Enzyme-like Activities of Nanozymes. To construct a series of bio-nano interfaces, we first prepared and characterized several representative nanozymes, including Fe_3O_4 NPs, Fe_3O_4@C NPs, Fe_3O_4@C NWs, and graphene oxide (GO) nanosheets. As illustrated in Figure 1A–D, the transmission electron microscopy (TEM) and atomic force microscopy (AFM) images revealed that four nanomaterials were in different dimensionalities ranging from zero-dimensional (0D) to one-dimensional (1D), and two-dimensional (2D). The core–shell nanostructure of Fe_3O_4@C NW has been further characterized by a scanning electron microscopy (SEM) image (Figure S1), which revealed that Fe_3O_4 NPs were encapsulated into the carbon shell layer. All four nanostructures were composed of one or two components

https://doi.org/10.1021/acsami.1c04241
ACS Appl. Mater. Interfaces 2021, 13, 21040–21050

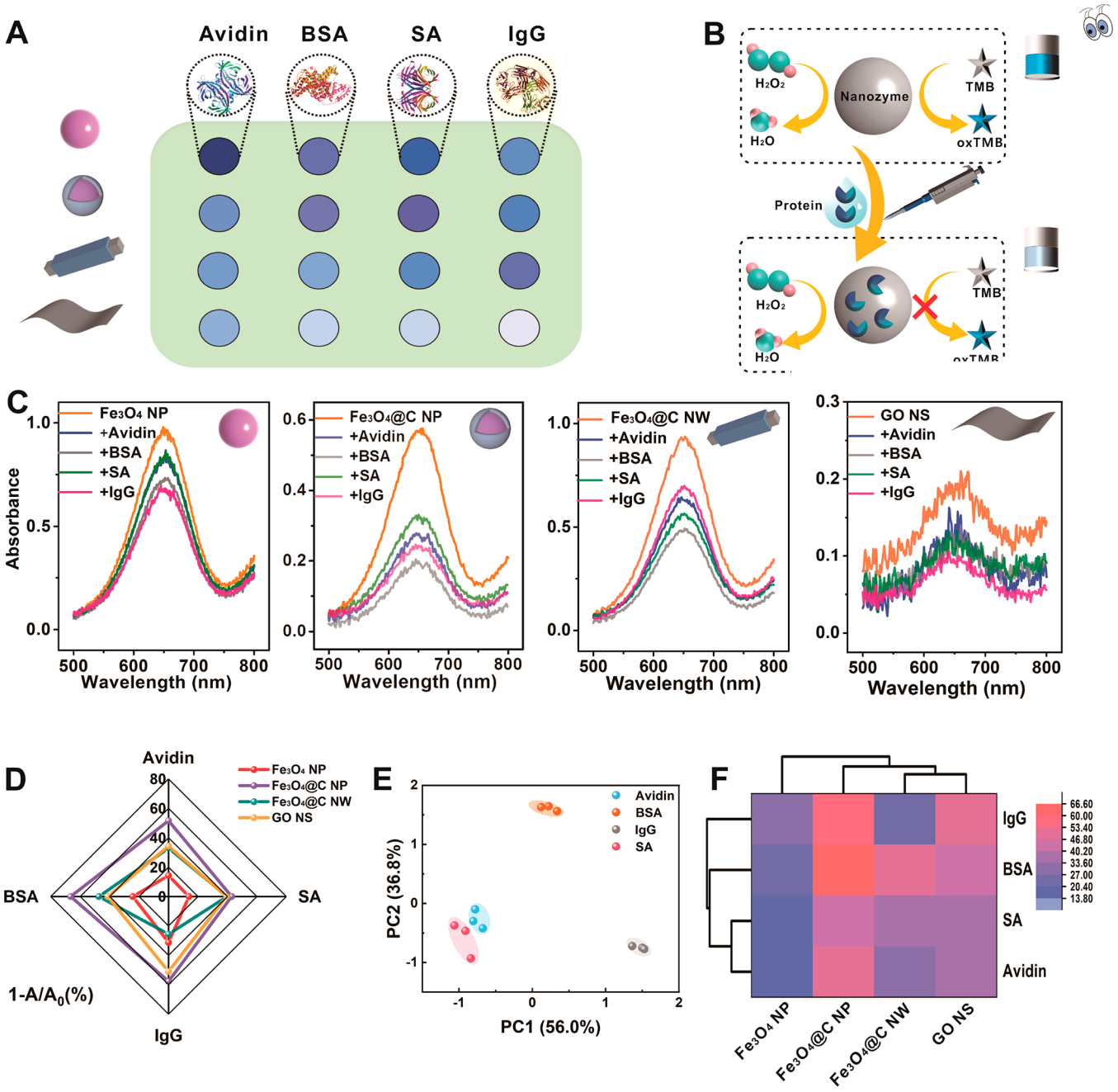

Figure 2. Interactions between nanozymes and proteins. (A) Schematic illustration of constructing a series of bio-nano interfaces on nanozymes using different proteins. (B) Scheme showing the absorption of protein to modulate the catalytic activities of nanozymes. (C) Typical UV−vis spectra of the peroxidase-like activities of protein-functionalized nanozymes. (D) Radar map for assessment of the signal suppression ratio of the peroxidase-like activities of the protein-functionalized nanozymes. (E) Canonical score plot for the first two factors of the colorimetric response patterns obtained from PCA analysis against four proteins. (F) Heat map derived from colorimetric response for four proteins. In this assay, 0.2 mg mL^{-1} protein was first incubated with 0.8 mg mL^{-1} nanozyme in PBS buffer. Then, the catalytic reaction was carried out by using a 20 μg mL^{-1} nanozyme/protein conjugate in 0.2 M HAc-NaAc (pH 4.0) containing 1 mM TMB and 5 mM H_2O_2.

of iron oxide and carbon, which were two typical compositions as enzyme mimics. To study the enzyme-mimicking properties, we employed classical catalytic reaction for a natural enzyme (e.g., horseradish peroxidase, HRP), in which the substrate TMB was catalyzed by H_2O_2 to its oxidized form with maximum absorbance at 652 nm. Figure 1E revealed that all four nanomaterials could effectively catalyze TMB into its blue oxidized form in the presence of H_2O_2, confirming their peroxidase-like activities. In comparison, we found that GO NS possessed the minimal activity, whereas the other three nanomaterials showed much higher activities. In addition, all four nanozymes followed typical Michaelis−Menten kinetics for the substrates of TMB and H_2O_2, respectively (Figure S2).[28,40,50] As indicated by the value of K_m (Figure 1F), Fe_3O_4@C NWs showed the highest activity to H_2O_2 and then Fe_3O_4@C NPs, which was 4277- and 83-fold compared to that of Fe_3O_4 NPs. In contrast, the K_m of GO NS to TMB was 3.1, 7.3, and 3.7 times lower than that of Fe_3O_4 NPs, Fe_3O_4@C NPs, and Fe_3O_4@C NWs, respectively, indicating that GO NS showed the maximum catalytic efficiency toward TMB.

https://doi.org/10.1021/acsami.1c04241
ACS Appl. Mater. Interfaces 2021, 13, 21040−21050

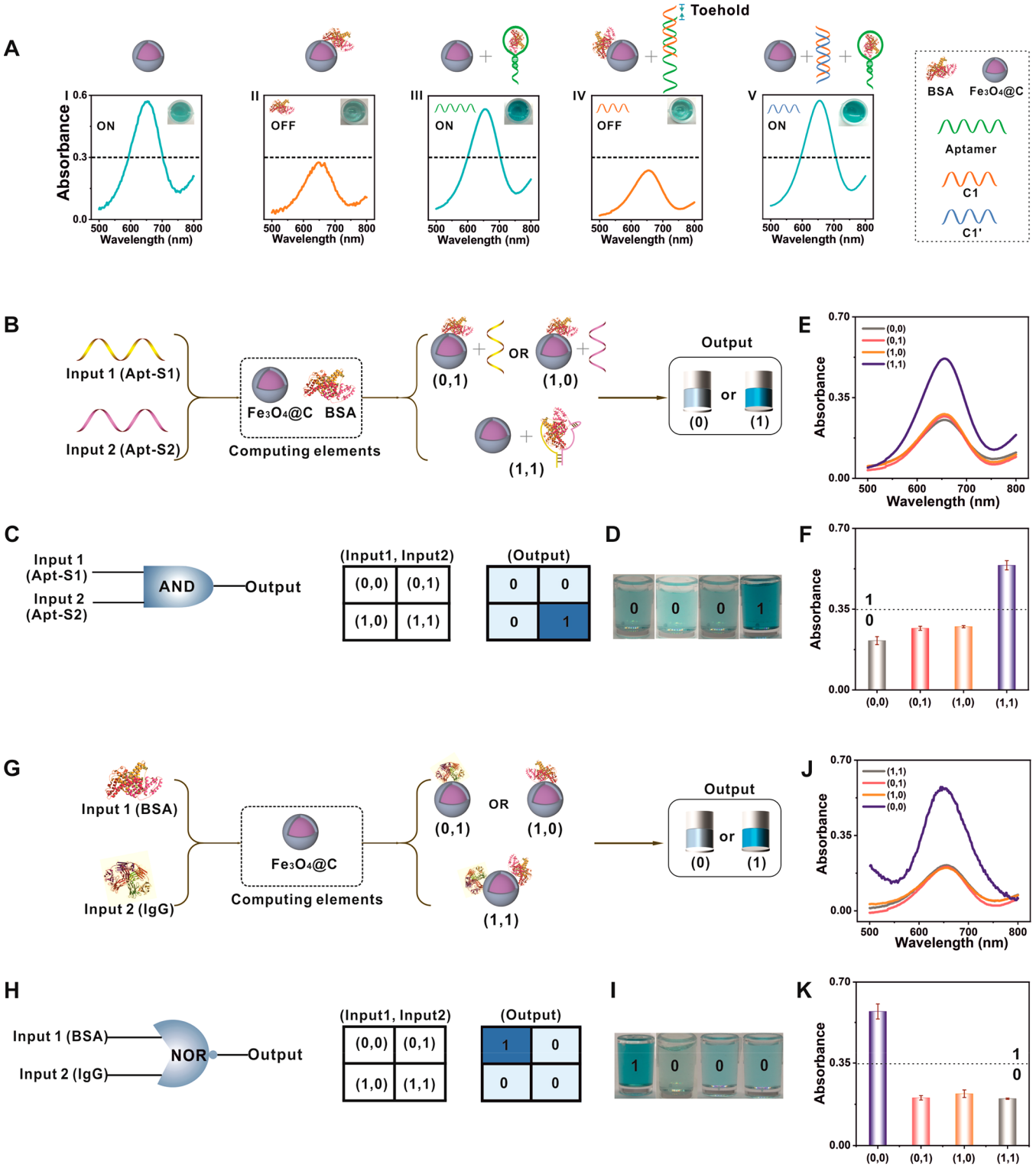

Figure 3. Biomolecular switching of nanocatalytic activities. (A) Schematic illustration and typical UV−vis spectra of switchable catalytic activities of Fe_3O_4@C NPs empowered by BSA, aptamer, lock DNA (C1), and key DNA (C1′). (B−K) Logic gate application. Schematic representations (B, G), truth table (C, H), photographs of reacted solution (D, I), and colorimetric responses (E, F, G, K) of AND and NOR logic gates with different combinations of inputs. In the incubation procedure, the concentrations of BSA, DNA, and Fe_3O_4@C NP were 0.2 mg mL^{-1}, 6 μM, and 0.8 mg mL^{-1}, respectively. The catalytic reaction was carried out by using 20 μg mL^{-1} bare/modified Fe_3O_4@C NP in 0.2 M HAc-NaAc (pH 4.0) containing 1 mM TMB and 5 mM H_2O_2. The error bars represent the standard deviation of three measurements.

Construction of Bio-Nano Interfaces on Nanozymes. In a typical process, immobilization of proteins has been widely regarded as a crucial step in sensor design. For example, avidin and SA as link biomolecules have been frequently attached to the surface of nanomaterials to conjugate antibody/enzyme via affinity interaction with biotin,[48] while BSA modification on the nano-interface can efficiently eliminate nonspecific binding in the preparation of capture surface and signaling probe.[51]

https://doi.org/10.1021/acsami.1c04241
ACS Appl. Mater. Interfaces 2021, 13, 21040−21050

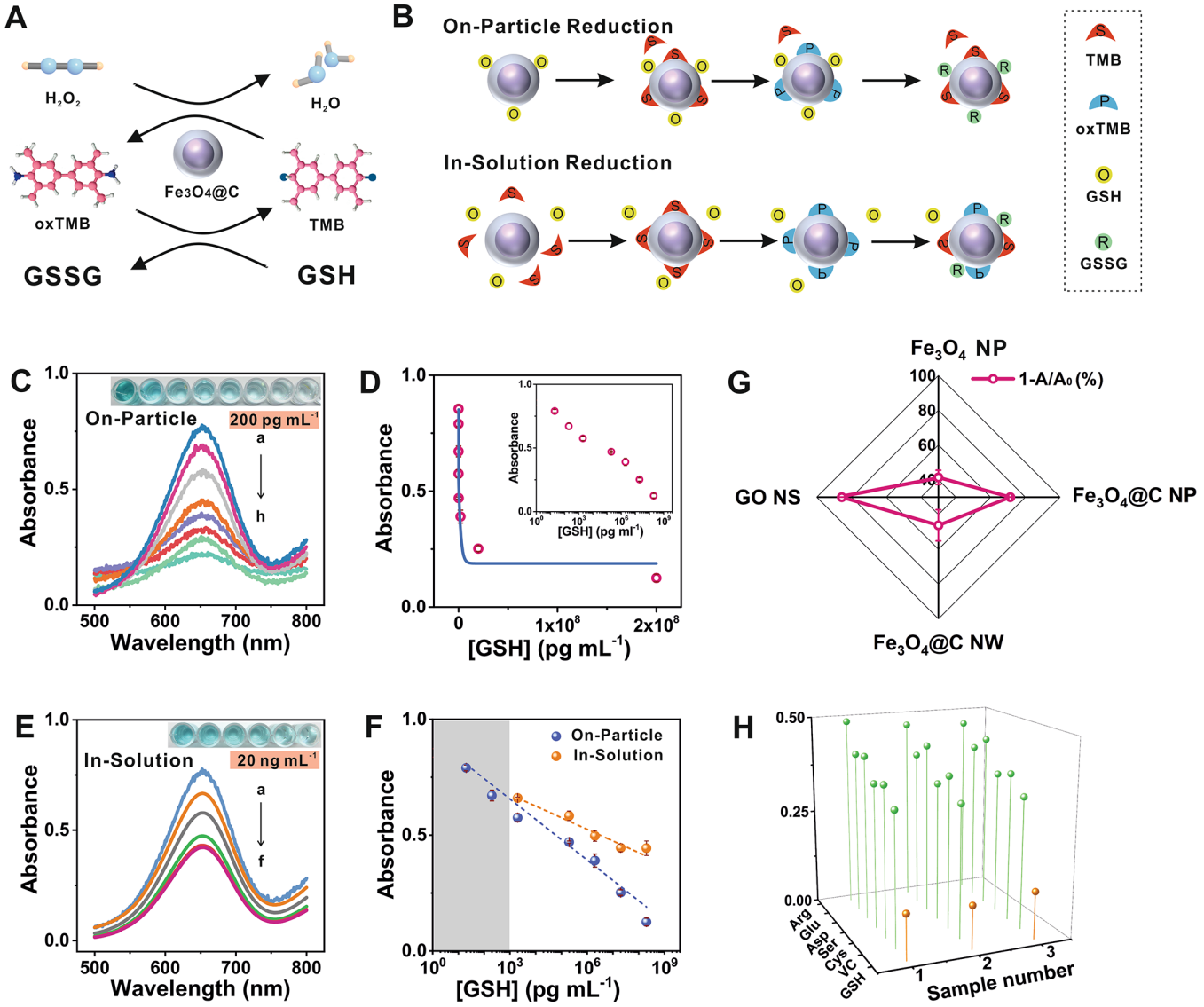

Figure 4. Ultrasensitive GSH biosensors. (A) Scheme for Fe_3O_4@C NP-based colorimetric assay for GSH detection. (B) Schematics for possible modes of on-particle reaction and in-solution reaction for GSH bioassays. (C) UV−vis spectra of the on-particle reaction-based sensor in response to different concentrations of GSH. From a to h: 0, 200 pg mL^{-1}, 2 ng mL^{-1}, 20 ng mL^{-1}, 200 ng mL^{-1}, 2 μg mL^{-1}, 20 μg mL^{-1}, and 200 μg mL^{-1}. Inset: photographs of their corresponding reacted solutions. (D) Scattered dot plot of absorbance signal at 652 nm vs GSH concentration. Inset: their corresponding logarithmic plot. (E) UV−vis spectra of the in-solution reaction-based sensor in response to different concentrations of GSH. From a to f: 0, 20 ng mL^{-1}, 200 ng mL^{-1}, 2 μg mL^{-1}, 20 μg mL^{-1}, and 200 μg mL^{-1}. Inset: photographs of their corresponding reacted solutions. (F) The linear relationship between the absorbance at 652 nm and the concentration of GSH. (G) Radar map for evaluation of the suppression of the peroxidase-like activity of four nanozymes by GSH based on on-particle method. (H) Selectivity of on-particle reaction-based biosensor toward potential interferences and GSH. The concentration of GSH was 0.2 mg mL^{-1}, and the concentrations of other interfering substrates were 4 mg mL^{-1}. When interacted with GSH, the concentration of Fe_3O_4@C NP was 0.8 mg mL^{-1}. The catalytic reaction was carried out by using 30 μg mL^{-1} nanozyme/protein conjugate in 0.2 M HAc-NaAc (pH 4.0) containing 1 mM TMB and 5 mM H_2O_2.

Moreover, the binding of protein antigen (e.g., IgG) on the surface is a central event in competitive immunoassay.[52] To comprehensively evaluate the influence of protein modification on nanozymes, four proteins with different roles in sensor design, including avidin, SA, BSA, and IgG, were selected as the model ligands for a proof-of-concept study. In the construction of bio-nano interfaces, we used direct immobilization through physical interaction that is the most commonly used strategy to fabricate biohybrid nanomaterials.

As shown in Figure 2A, proteins bearing varying sizes and charges showed differential affinities to the surface of nanomaterials, resulting in altered catalytic behaviors of nanozymes and color changes toward TMB oxidation. We reasoned that the absorption of protein prevented the interaction between the nanomaterial and the substrate of TMB and thus led to a modulation of the catalytic efficiency of the nanozyme (Figure 2B). In a typical procedure, each protein with the same concentration was first incubated with the nanomaterials in phosphate buffer saline (PBS, pH 7.4) and then reacted with TMB in the presence of H_2O_2. Figure 2C illustrates the absorbance signals recorded by UV−vis spectra. As a result, the colorimetric response at 652 nm was weakened with varying degrees with the addition of protein. The signal suppression ratios of the peroxidase-like activities (defined as $1 - A/A_0$) catalyzed by protein-functionalized nanozymes were evaluated and are summarized in Figure 2D. Notably, the

https://doi.org/10.1021/acsami.1c04241
ACS Appl. Mater. Interfaces 2021, 13, 21040−21050

functionalization of protein showed a maximum inhibition on the catalytic activity of Fe_3O_4@C NP, while the peroxidase-like activity of Fe_3O_4 NP was mostly retained.

Taking advantage of the differential regulation on the catalytic activities of the four nanozymes by different proteins, we constructed an array-based sensor for multiplex protein identification. To assess the discrimination ability against proteins, the colorimetric patterns were analyzed by principal component analysis (PCA), which converted the data matrix (4 receptors × 4 analytes × 3 replicates) into a 2D canonical score plot. As shown in Figure 2E, the canonical patterns were clustered into four separate clusters corresponding to four proteins, suggesting that proteins were effectively discriminated from each other without cross-classification. Moreover, the narrow distances between three replicated points in each cluster revealed excellent reproducibility of the measurements. The heat map demonstrated satisfactory differentiability of the four recognizing receptors to four proteins (Figure 2F). More importantly, this sensor array demonstrated a favorable sensitive identification of protein at nanomolar level. For instance, a canonical score plot for the first two factors of colorimetric response patterns was obtained from PCA analysis against various concentrations of BSA ranging from 100 nM to 3 μM (Figure S3A). In addition, the linear dose−response curve revealed the homogeneous and stable interaction between nanozyme and protein (Figure S3B). Taken together, the proposed sensor array demonstrated a good capability in correctly distinguishing proteins with high accuracy.

Biomolecular Switches of Nanocatalytic Activities. Given the maximum catalytic modulation on Fe_3O_4@C NP by BSA among all bio-nano systems, we sought to establish biomolecular switches of the catalytic activities using this system. In the initial state (ON), the Fe_3O_4@C NP showed an excellent peroxidase-like activity (I, Figure 3A). After the introduction of BSA, the catalytic activity of Fe_3O_4@C NP was obviously inhibited and switched to the "OFF" state (II, Figure 3A). In the presence of BSA specific aptamer,[53] the high binding affinity of BSA and its aptamer led to reactivation of the catalytic activity of Fe_3O_4@C NP (III, Figure 3A). To implement a switch-off operation, a lock DNA strand (C1) with an 8 nt toehold was introduced which hybridized with the aptamer to release BSA (IV, Figure 3A). In turn, a key DNA strand (C1′) that fully matched the lock strand was allowed to trigger the toehold-mediated strand displacement for the switch-on operation (V, Figure 3A). Colorimetric signal switches confirmed the catalytic changes of Fe_3O_4@C NPs triggered by BSA, aptamer, and lock and key DNA (Figure S4).

Having implemented the biomolecular switches of nanocatalytic activity, we then built Boolean logic calculation systems on the basis of the bio-nano interface of Fe_3O_4@C NP. In the AND logic gate, Fe_3O_4@C NP and BSA served as gate structure, and two split aptamers of BSA (Apt-1 and Apt-2) were designed as two inputs (Figure 3B, C). When no input or either one input was presented to the gate structure (input = [0, 0], [1, 0], or [0, 1]), a low level of absorbance at 652 nm could be observed (Figure 3E,F), confirming a low catalytic activity of Fe_3O_4@C NP (output = 0). In the presence of both two inputs (input = [1, 1]), split aptamers recombined and competitively bound with BSA, which resulted in a large colorimetric signal as well as dark blue reaction solution (Figure 3D), confirming the recovery of high catalytic activity of Fe_3O_4@C NP (output = 1). For the NOR logic gate, Fe_3O_4@C NP was employed as the computing element, and two proteins (BSA and IgG) were designed as two inputs (Figure 3G,H). In the absence of any input (input = [0, 0]), the initial state of the logic gate exhibited high catalytic activity (output = 1); otherwise, when either one or two inputs were present (input = [1, 0], [0, 1], or [1, 1]), the absorbance level was low (output = 0) (Figure 3J,K). These outputs were also verified by the color of corresponding reacted solutions by the naked eye (Figure 3I), which well matched the designed logic operation. The logic platform provided a label-free and visible biocomputing concept by using the biohybrid nanozyme, which held a great promise in intelligent clinical diagnosis and on-site detection.

On-Particle Reaction for Detection of GSH. GSH, as an important intracellular antioxidant, plays a crucial role in cellular functions in defensing free radicals and toxins and keeping exogenous antioxidants in reduced forms.[54,55] Also, it is employed as a therapeutic drug for treatment of convulsions and epilepsy. Therefore, quantitative determination of GSH in living being systems and pharmaceuticals is of great significance. Given the crucial role of a bio-nano interface in regulating molecular interactions, we developed an on-particle reaction strategy for colorimetric detection of GSH with interfacial microenvironments. Figure 4A illustrates a schematic representation of colorimetric detection of GSH based on the peroxidase-like activity of Fe_3O_4@C NP. Briefly, when GSH was introduced, the blue color fading occurred into the TMB-H_2O_2 chromogenic system. Also, the color change of the solution was concentration-dependent and thus allowed the quantitative analysis of GSH. As shown in Figure 4B, the reaction pathway for on-particle reaction, in which GSH first absorbed and concentrated on the surface, enhanced the reduction ability toward oxidized TMB (TMBox), which differed significantly from that in bulk solution. Because of the high affinity between GSH and the surface of Fe_3O_4@C NP, the exposed surface was blocked, resulting in binding hindrance of TMB substrate. Meanwhile, the absorption of GSH could accelerate the involved reactions due to localized interfacial interactions and "concentric" effect.

We next interrogated the analytical performance of on-particle reaction-based colorimetric biosensors to detect GSH. Figure 4C shows a series of typical UV−vis spectra in response to different concentrations ranging from 200 pg mL^{-1} to 200 μg mL^{-1}. It was observed that the absorbance at 652 nm showed a gradual weakening with an increasing concentration of GSH, in accordance with the color change of reacted solutions (Figure 4C, inset). The colorimetric signal was plotted as a monotonic function of GSH concentration spanning 7 orders of magnitude (Figure 4D). Additionally, there was a linear relationship between the absorbance and the logarithm of concentration with a regression equation (A = 0.91957 − 0.08788 log C_{GSH}, R^2 = 0.96218) (Figure 4D, inset). For in-solution reaction-based colorimetric biosensor, it exhibited a dynamic response range from 20 ng mL^{-1} to 20 μg mL^{-1}, with a linear regression equation (A = 0.82572 − 0.05015 log C_{GSH}, R^2 = 0.98093) (Figure 4E). By contrast, it was found that the sensitivity of the on-particle reaction-based biosensor surpassed that of in-solution reaction by 2 orders of magnitude (Figure 4F), indicating that the bio-nano interface could effectively improve the sensitivity of the GSH bioassay. Two proposed sensors achieved limit of detections as low as 200 pg mL^{-1} (650 pM, on-particle) and 20 ng mL^{-1} (65 nM, in-solution), respectively. Such an ultrahigh sensitivity of on-particle based GSH biosensor was comparable to or even

https://doi.org/10.1021/acsami.1c04241
ACS Appl. Mater. Interfaces 2021, 13, 21040−21050

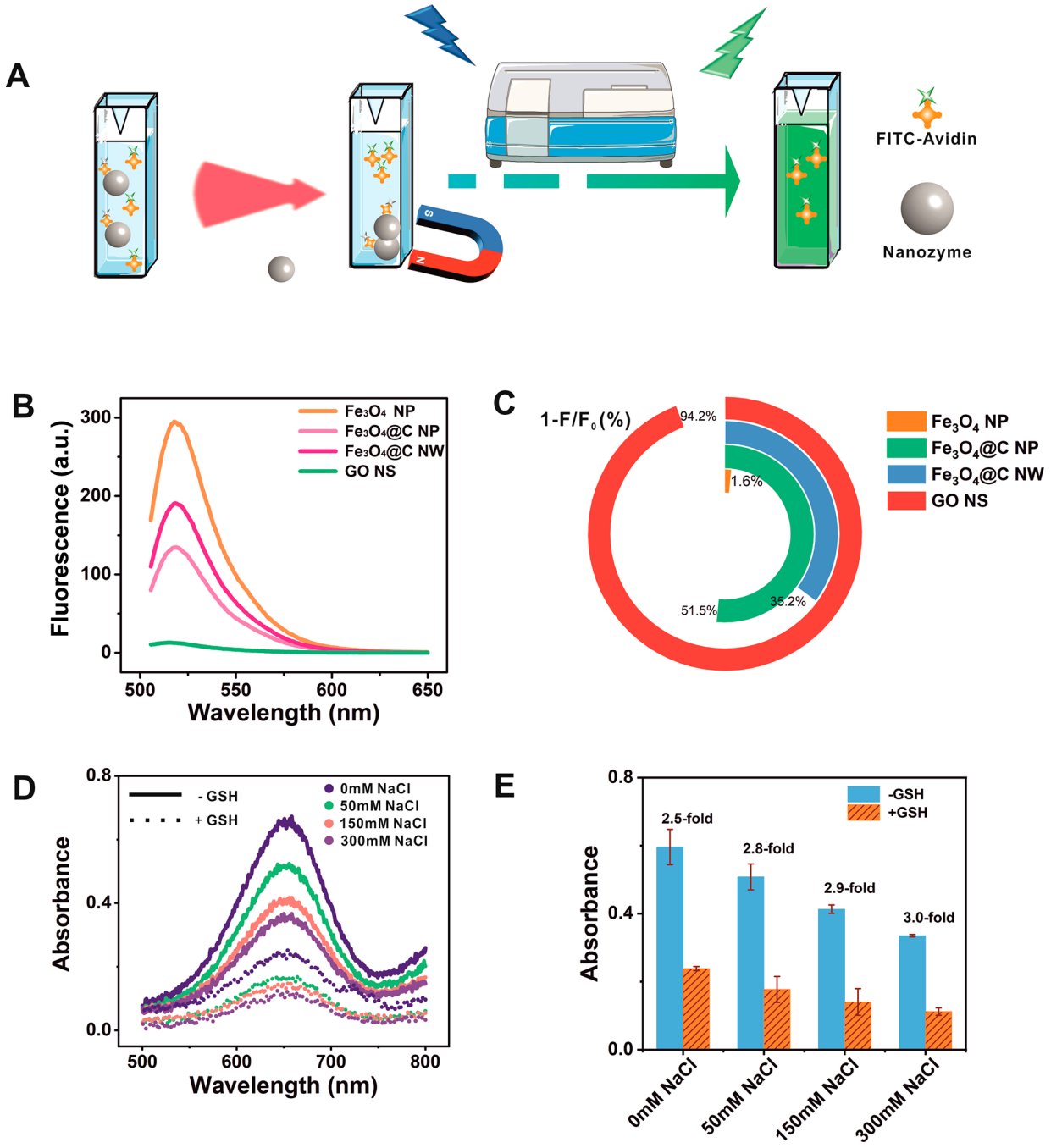

Figure 5. (A) Schematic illustration of the fluorescent method for protein quantification. (B, C) Fluorescence spectra (B) and quenching efficiency (C) obtained from four nanosystems. (D, E) UV−vis spectra (D) and comparisons (E) of the catalytic oxidation of TMB in the absence and presence of GSH in different concentrations of NaCl. In fluorescence measurement, 0.2 mg mL^{-1} FITC-avidin was incubated with 0.8 mg mL^{-1} nanozyme in PBS buffer. In salt influence test, 0.2 mg mL^{-1} GSH and 0.8 mg mL^{-1} Fe_3O_4@C NP were used in incubation. Then, the catalytic reaction was carried out by using 20 μg mL^{-1} nanozyme/protein conjugate in 0.2 M HAc-NaAc (pH 4.0) containing 1 mM TMB and 5 mM H_2O_2.

superior to that of previous colorimetric biosensors for GSH (Table S2). In addition to ultrahigh sensitivity, our proposed on-particle based GSH biosensor also exhibited several advantages. Significant qualities of this biosensing system are simplicity and easy-to-use, and not requiring complex and time-consuming experimental procedures. Importantly, biomolecular detection can be accomplished by visual observation. In addition, this sensor system is label-free and cost-effective, which does not need costly manipulations, such as chemical synthesis or nanoparticle modification.

Besides that, the suppressions of the peroxidase-like activities of four nanozymes by GSH are also illustrated in Figure 4G. As a result, both Fe_3O_4@C NP and GO NS demonstrated high inhibition efficiencies of about 80%, whereas there was a low inhibition efficiency of less than 50% for either Fe_3O_4 NP or Fe_3O_4@C NW. Besides that, it was also worth noting that the inhibition efficiency of the on-particle reaction-based GSH biosensor was apparently higher than that of the in-solution reaction-based counterpart under the same conditions, reconfirming the significance of the bio-nano interface in a biosensing platform. To assess the

https://doi.org/10.1021/acsami.1c04241
ACS Appl. Mater. Interfaces 2021, 13, 21040−21050

specificity of our on-particle based GSH sensor, we carried out control experiments using potential interference of a component in body fluid, including several amino acids, some reductive substrates, including L-aspartic acid (Asp), L-glutamic acid (Glu), L-serine (Ser), L-arginine (Arg), L-cysteine (Cys), and vitamin C (VC). As shown in Figure 4H, we found that the introduction of GSH caused a dramatic decrease in the absorbance, whereas the other interferences gave rise to insignificant effects on colorimetric signals, even with a 20-fold excess relative to GSH. Furthermore, the mixture with other proteins, e.g., glucose oxidase (GOx), biotin, and concanavalin (ConA), produced slight influence on the colorimetric response (Figure S5). This suggested that our proposed sensor possessed satisfactory discrimination between GSH and other biological components.

Mechanism of Nanozyme-Biomolecue Interactions. It has revealed that proteins showed modulation of the peroxidase-mimicking activity of nanomaterials, which resulted in different degrees of reduction of the colorimetric responses of different nanozymes. To get the insights of the mechanism of the interactions between protein and nanozyme, we quantitatively measured the protein densities on the surface of nanomaterials using a fluorescent method. Considering avidin as a moderate catalytic regulator for four nanozymes, we selected fluorescein isothiocyanate (FITC)-labeled avidin, as the model protein for fluorescence studies. After interacting with nanozyme, the unbound FITC-avidin was separated in the supernatant under an external magnetic field, and then its fluorescence intensity was determined (Figure 5A). Figure 5B displays the fluorescence intensity for the free FITC-avidin obtained from four nanozymes. The fluorescence of free FITC-avidin in the sample of Fe_3O_4 NP was well maintained in a high level, whereas that for GO NS was nearly totally quenched with a relatively low response. Quenching efficiency (η) was employed to present the quenching abilities of nanozyme for FITC-avidin, which was calculated as $1 - F/F_0$, where F_0 and F are the fluorescence intensities at 525 nm in the absence and presence of nanozyme, respectively. As presented in Figure 5C, the quenching efficiency caused by GO NS was as high as 94%, implying the strong GO-protein binding and the resulting high absorption of protein on the surface of GO NS. In a sharp contrast, Fe_3O_4 NP quenched the fluorescence with a very low efficiency of 1.6% due to a weak interaction between Fe_3O_4 NP and protein. In addition, 52% and 35% fluorescence were quenched by Fe_3O_4@C NP and Fe_3O_4@C NW, respectively, both of which suggested moderate absorption efficiency for protein. The amount of nanozyme, surface area, and surface density for four nanosystems are listed in Table S3. Both Fe_3O_4 NP and Fe_3O_4@C NW possessed a surface area of more than 100 $m^2\ g^{-1}$, which were much larger than that of Fe_3O_4@C NP and GO NS. After the addition of protein, similar average surface densities were calculated for both Fe_3O_4@C NP and GO NS systems, which were around 10- and 100-fold higher than that of Fe_3O_4@C NW and Fe_3O_4 NP, respectively. This phenomenon suggested a high absorption efficiency of protein on the surface of either Fe_3O_4@C NP or GO NS, which explained their significant inhibition ratios of the catalytic activities of Fe_3O_4@C NP and GO NS (Figure 2D). By the same token, the ultralow surface density of protein on Fe_3O_4 NP was considered to be related to a slight change of its catalytic activity. We speculated that the bound protein molecules occupied the room to anchor and shielded the nanozyme surface, which might block the surface accessibility of the peroxidase substrate and thus gave rise to an inhibition of peroxidase-like activity.

Next, we studied the effect of ionic strength on the interactions between nanozymes and biomolecules. The peroxidase-like activities of nanozymes were investigated in the absence and presence of biomolecules with different concentrations of salt. In the absence of biomolecules, the peroxidase-like activities of four nanozymes exhibited varying degrees of decrease with increasing salt concentrations (Figure S6). Particularly, it demonstrated the maximum decrease of the absorbance for Fe_3O_4@C NP. When biomolecule (e.g., GSH) was added, the higher salt concentration led to an enhanced inhibition ratio of the peroxidase-like activity of Fe_3O_4@C NP (Figure 5D,E). From ζ-potential measurements, four nanozymes carried a negative charge in physiological pH (Table S4). GSH, SA, and BSA were negatively charged in the same buffer (Table S5). As salt was usually used to screen the charge repulsion in aqueous nanosystems, thus electrostatic force might contribute to the bio-nano interactions.[47] In other examples, avidin and IgG carried a positive charge at pH 7.4, which favored the electrostatic attractive binding with negatively charged nanozyme.[56] In short, higher salt concentration brought about more impact on the catalytic inhibition of bio-nano interfaces, and electrostatic force might play an important role in the bio-nano interactions.

Considering that four nanozymes with diverse shapes possessed different surface curvatures, the shape was also taken into account as an influencing factor to analyze. As is known to all, the 0D NPs have maximum curvature and energy, and then 1D NWs, and last the 2D NSs. The biomolecules need to consume higher energy to bend in the direction of the imposed curvature on the spherical surface for 0D NPs, which made the adsorption on Fe_3O_4 NP lower than on nanowires and nanosheets. For Fe_3O_4@C NPs, biomolecules might bind on the surface via different interaction forces, such as hydrogen bonding, electrovalent bond, van der Waals forces, and hydrophobicity, which contributed to the highest absorption of this nanozyme among the four nanosystems. However, the detailed mechanism is still unclear and needs to be in-depth explored.

CONCLUSION

In summary, four types of nanozymes from 0D to 2D and their interactions with biomolecules were systematically studied for better understanding their roles and rational biosensing design. The colorimetric assays revealed that the modification of proteins caused the catalytic regulation behaviors of nanozymes. As a result, the catalytic activity of Fe_3O_4@C NP was maximally inhibited, whereas that of Fe_3O_4@C NP mostly remained. What's more, the nanozyme-based sensor array showed good identification for multiplex proteins, including avidin, SA, BSA, and IgG. On the basis of the highest inhibition of BSA on Fe_3O_4@C NP, the catalytic activity of Fe_3O_4@C NP could be switched ON/OFF empowered by BSA, aptamer, and toehold DNA, allowing the establishment of Boolean logic calculations (AND and NOR) in response to DNA and protein stimuli that converted to the color change of corresponding reacted solutions. Given the "concentric" effect of the bio-nano interface, an on-particle reaction strategy for colorimetric detection of GSH has been proposed, which demonstrated a wide dynamic range from 200 pg mL^{-1} to 200 $\mu g\ mL^{-1}$ spanning 7 orders of magnitude, as well as good discrimination from other potential interferences. Worth of

https://doi.org/10.1021/acsami.1c04241
ACS Appl. Mater. Interfaces 2021, 13, 21040−21050

noting, the on-particle reaction-based GSH sensor exhibited an ultrahigh sensitivity down to 200 pg mL^{-1}, which exceeded that of the in-solution reaction-based sensor by 2 orders of magnitude. More importantly, the mechanism of the interactions between nanozymes and biomolecules was carefully explored by analyzing the related influencing factors. The surface coverage of biomolecules, salt concentration, and the curvature of nanozymes have been proved highly associated with the catalytic modulation. We envisage that this work can provide guidance for better choice of nanozymes and the elaborate design of biosensors for molecular diagnosis and in vivo sensing.

EXPERIMENTAL SECTION

Materials and Chemicals. The aptamer and DNA oligonucleotides were synthesized by Sangon Biotech Co., Ltd. (Shanghai, China, and used without further purification. All sequences of the oligonucleotides are listed in Table S1. GO NSs were purchased from Nanjing XFNANO Materials Tech Co., Ltd. (Nanjing, China). Avidin, SA, BSA, and IgG were obtained from Sangon Biotech Co., Ltd. (Shanghai, China). GSH and 30% H_2O_2 were purchased from Shanghai Titan Scientific Co., Ltd. (Shanghai, China). TMB was purchased from Sinopharm Chemical Reagent Co., Ltd. (Shanghai, China). All chemicals were of analytical reagent grade and used without further purification. Ultrapure water with a resistivity of 18 $M\Omega \cdot cm^{-1}$ was used in the assays.

Assay of the Peroxidase-like Activities of Nanozyme. The peroxidase-like activities of nanozymes were studied by a TMB/H_2O_2 reaction system. Briefly, 6 μL of 1 mg mL^{-1} nanozyme, 15 μL of 20 mM TMB, and 15 μL of 0.1 M H_2O_2 were added into 264 μL of HAc-NaAc buffer (0.2 M, pH 4.0). The resulting mixture reacted for 10 min at room temperature, and then the nanozyme was removed under a magnetic field or by centrifugation. Finally, the supernatant was monitored on a UV−vis spectrometer using a wavelength scanning method.

Investigation of Interactions between Nanozymes and Proteins. First, 25 μL of 1 mg mL^{-1} protein was mixed with 100 μL of 1 mg mL^{-1} nanozyme in a 1×PBS solution, and the resultant mixture reacted overnight at 37 °C under slightly stirring. The nanozyme/protein conjugate was washed with 1×PBS for three times. Then, 6 μL of 1 mg mL^{-1} of nanozyme/protein conjugate was added into the HAc-NaAc buffer solution containing 1 mM TMB and 5 mM H_2O_2. The mixture further reacted for 10 min at room temperature, and the supernatant was transferred to a quartz cell and used for spectroscopic measurements.

Construction of Logic Gates. For AND logic gate operations, input DNAs (Apt-S1 and Apt-S2) were added to BSA, and then incubated for 30 min at 37 °C. Then, the above mixture reacted with Fe_3O_4@C NP overnight at 37 °C. For NOR logic gate operations, input proteins (BSA and IgG) were introduced to Fe_3O_4@C NP with an incubation at 37 °C overnight. The following steps were performed as described in Assay of the Peroxidase-like Activities of Nanozyme section. The logic gate against different inputs and their biological outputs were characterized by the corresponding colorimetric signal as well as the color change of the catalytic oxidation of TMB.

Colorimetric Determination of GSH. For the on-particle reaction-based GSH sensor, GSH with different concentration was added to 1 mg mL^{-1} Fe_3O_4@C NP in 1×PBS solution, and reacted for 2 h at room temperature which made GSH fully absorb on the surface of Fe_3O_4@C NP. After centrifugation, a 9 μL volume of 1 mg mL^{-1} Fe_3O_4@C NP/GSH conjugate was added to HAc-NaAc buffer solution (0.2 M, pH 4.0) containing 1 mM TMB and 5 mM H_2O_2, and then reacted for 10 min. For the in-solution reaction-based GSH sensor, GSH with different concentrations was added to HAc-NaAc buffer solution (0.2 M, pH 4.0) containing 30 μg mL^{-1} Fe_3O_4@C NP, 1 mM TMB, and 5 mM H_2O_2, and reacted for 10 min. Finally, the chromogenic TMB solution was monitored by spectroscopic measurements.

Fluorescence Assay. 25 μL of 1 mg mL^{-1} FITC-avidin was added to 100 μL of 1 mg mL^{-1} nanozyme. The mixture reacted at 37 °C overnight with slight stirring, and washed with 1×PBS for three times. The supernatant was measured on a fluorescence spectroscopy (Hitachi, Japan) with an excitation/emission wavelength of 496/518 nm.

ASSOCIATED CONTENT

Supporting Information

The Supporting Information is available free of charge at https://pubs.acs.org/doi/10.1021/acsami.1c04241.

Synthesis of nanomaterials, construction of biomolecular switches, apparatus, and characterization, DNA sequences, SEM image, steady-state kinetic assays, identification of BSA at different concentrations, colorimetric signal switches, selectivity of on-particle GSH sensor in mixture, salt influence on the peroxidase-like activities of four nanozymes (PDF)

AUTHOR INFORMATION

Corresponding Authors

Na Lu − *School of Materials Engineering, Shanghai University of Engineering Science, Shanghai 201620, China;* orcid.org/0000-0001-5771-247X; Email: nlu2014@163.com

Zisheng Tang − *Department of Endodontics, Shanghai Ninth People's Hospital, Shanghai Jiao Tong University School of Medicine, Shanghai 200011, China; College of Stomatology, Shanghai Jiao Tong University, Shanghai 200011, China; National Center for Stomatology, Shanghai 200011, China; National Clinical Research Center for Oral Diseases, Shanghai 200011, China; Shanghai Key Laboratory of Stomatology, Shanghai 200011, China;* Email: tangzisheng163@163.com

Min Zhang − *College of Chemistry and Chemical Engineering, Shanghai University of Engineering Science, Shanghai 201620, China;* orcid.org/0000-0002-5242-0491; Email: zhangmin@sues.edu.cn

Authors

Jie Li − *School of Materials Engineering, Shanghai University of Engineering Science, Shanghai 201620, China*

Suping Han − *Department of Pharmacy, Shandong Medical College, Jinan 250002, China*

Xuemei Li − *School of Materials Engineering, Shanghai University of Engineering Science, Shanghai 201620, China*

Mengqin Wang − *School of Materials Engineering, Shanghai University of Engineering Science, Shanghai 201620, China*

Mengchao Cai − *School of Materials Engineering, Shanghai University of Engineering Science, Shanghai 201620, China*

Complete contact information is available at: https://pubs.acs.org/10.1021/acsami.1c04241

Notes

The authors declare no competing financial interest.

ACKNOWLEDGMENTS

This work was financially supported by the National Key Research and Development Program (2016YFA0201200), the National Natural Science Fund of China (81974317, 82071105, 81870749, and 21934007), the Program for Professor of Special Appointment (Eastern Scholar) at Shanghai Institutions of Higher Learning, the Talent Program

of Shanghai University of Engineering Science, Cross-disciplinary Research Fund of Shanghai Ninth People's Hospital, Shanghai Jiao Tong University School of Medicine (JYJC202006), and Shandong Provincial Medical and Health Science and Technology Development Plan Program (2020-11001041).

REFERENCES

(1) Nam, J.-M.; Thaxton, C. S.; Mirkin, C. A. Nanoparticle-Based Bio-Bar Codes for the Ultrasensitive Detection of Proteins. *Science* **2003**, *301*, 1884−1886.
(2) Xie, P.; Xiong, Q.; Fang, Y.; Qing, Q.; Lieber, C. M. Local Electrical Potential Detection of DNA by Nanowire-Nanopore Sensors. *Nat. Nanotechnol.* **2012**, *7*, 119−125.
(3) Lu, N.; Gao, A.; Dai, P.; Song, S.; Fan, C.; Wang, Y.; Li, T. CMOS-Compatible Silicon Nanowire Field-Effect Transistors for Ultrasensitive and Label-Free MicroRNAs Sensing. *Small* **2014**, *10*, 2022−2028.
(4) Quesada-González, D.; Merkoçi, A. Nanomaterial-Based Devices for Point-of-Care Diagnostic Applications. *Chem. Soc. Rev.* **2018**, *47*, 4697−4709.
(5) Li, Q.; Lu, N.; Wang, L.; Fan, C. Advances in Nanowire Transistor-Based Biosensors. *Small Methods* **2018**, *2*, 1700263.
(6) Li, Z.; Wang, C.; Li, J.; Zhang, J.; Fan, C.; Willner, I.; Tian, H. Functional DNA Structures and Their Biomedical Applications. *CCS Chemistry* **2020**, *2*, 707−728.
(7) Kwon, P. S.; Ren, S.; Kwon, S. J.; Kizer, M. E.; Wang, X. Designer DNA Architecture Offers Precise and Multivalent Spatial Pattern-Recognition for Viral Sensing and Inhibition. *Nat. Chem.* **2020**, *12*, 26−35.
(8) Zhu, S.; Meng, Q.; Wang, L.; Zhang, J.; Song, Y.; Jin, H.; Zhang, K.; Sun, H.; Wang, H.; Yang, B. Highly Photoluminescent Carbon Dots for Multicolor Patterning, Sensors, and Bioimaging. *Angew. Chem.* **2013**, *125*, 4045−4049.
(9) Peng, F.; Su, Y.; Zhong, Y.; Fan, C.; Lee, S.-T.; He, Y. Silicon Nanomaterials Platform for Bioimaging, Biosensing, and Cancer Therapy. *Acc. Chem. Res.* **2014**, *47*, 612−623.
(10) Yang, H.; Li, R.; Zhang, Y.; Yu, M.; Wang, Z.; Liu, X.; You, W.; Tu, D.; Sun, Z.; Zhang, R.; et al. Colloidal Alloyed Quantum Dots with Enhanced Photoluminescence Quantum Yield in the NIR-II Window. *J. Am. Chem. Soc.* **2021**, *143*, 2601−2607.
(11) Lu, N.; Wang, L.; Lv, M.; Tang, Z.; Fan, C. Graphene-Based Nanomaterials in Biosystems. *Nano Res.* **2019**, *12*, 247−264.
(12) Chao, J.; Wang, J.; Wang, F.; Ouyang, X.; Kopperger, E.; Liu, H.; Li, Q.; Shi, J.; Wang, L.; Hu, J.; et al. Solving Mazes with Single-Molecule DNA Navigators. *Nat. Mater.* **2019**, *18*, 273−279.
(13) Ren, S.; Wang, J.; Song, C.; Li, Q.; Yang, Y.; Teng, N.; Su, S.; Zhu, D.; Huang, W.; Chao, J.; Wang, L.; Fan, C. Single-Step Organization of Plasmonic Gold Metamaterials with Self-Assembled DNA Nanostructures. *Research* **2019**, *2019*, 743580.
(14) Dunn, B.; Kamath, H.; Tarascon, J.-M. Electrical Energy Storage for the Grid: A Battery of Choices. *Science* **2011**, *334*, 928−935.
(15) Lin, D.; Liu, Y.; Cui, Y. Reviving the Lithium Metal Anode for High-Energy Batteries. *Nat. Nanotechnol.* **2017**, *12*, 194−206.
(16) Guo, Y.; Cao, Y.; Chen, Z.; Li, R.; Gong, W.; Yang, W.; Zhang, Q.; Wang, H. Fluorinated Metal-Organic Framework as Bifunctional Filler Toward Highly Improving Output Performance of Triboelectric Nanogenerators. *Nano Energy* **2020**, *70*, 104517.
(17) Zhang, M.; Ling, Y.; Liu, L.; Xu, J.; Li, J.; Fang, Q. Carbon Supported PdNi Alloy Nanoparticles on SiO_2 Nanocages with Enhanced Catalytic Performance. *Inorg. Chem. Front.* **2020**, *7*, 3081−3091.
(18) Zong, S.; Huang, S.; Shi, X.-R.; Sun, C.; Xu, S.; Ma, P.; Wang, J. Impact of Linker Functionalization on the Adsorption of Nitrogen-Containing Compounds in HKUST-1. *Dalton Trans.* **2020**, *49*, 12610−12621.
(19) Zheng, J.; Zhang, M.; Miao, T.; Yang, J.; Xu, J.; Alharbi, N. S.; Wakeel, M. Anchoring Nickel Nanoparticles on Three-Dimensionally Macro-/Mesoporous Titanium Dioxide with A Carbon Layer from Polydopamine Using Polymethylmethacrylate Microspheres as Sacrificial Templates. *Mater. Chem. Front.* **2019**, *3*, 224−232.
(20) He, J.; Ji, W.; Yao, L.; Wang, Y.; Khezri, B.; Webster, R. D.; Chen, H. Strategy for Nano-Catalysis in a Fixed-Bed System. *Adv. Mater.* **2014**, *26*, 4151−4155.
(21) Zhang, Y.; Shi, X.-R.; Sun, C.; Huang, S.; Duan, Z.; Ma, P.; Wang, J. CO Oxidation on Ni-Based Single-Atom Alloys Surfaces. *Mol. Catal.* **2020**, *495*, 111154.
(22) Li, X.; Huang, X.; Xi, S.; Miao, S.; Ding, J.; Cai, W.; Liu, S.; Yang, X.; Yang, H.; Gao, J.; et al. Single Cobalt Atoms Anchored on Porous N-Doped Graphene with Dual Reaction Sites for Efficient Fenton-Like Catalysis. *J. Am. Chem. Soc.* **2018**, *140*, 12469−12475.
(23) Zhang, M.; Ding, L.; Zheng, J.; Liu, L.; Alsulami, H.; Kutbi, M. A.; Xu, J. Surface Modification of Carbon Fibers with Hydrophilic Fe_3O_4 Nanoparticles for Nickel-Based Multifunctional Composites. *Appl. Surf. Sci.* **2020**, *509*, 145348.
(24) Nanoscale Engineering for Sustainable Catalysis. *Nat. Nanotechnol.* **2021**, *16*, 117..
(25) Shi, X.-R.; Huang, S.; Huang, Y.; Zhang, Y.; Zong, S.; Xu, S.; Chen, Y.; Ma, P. Atomic Structures and Electronic Properties of Ni or N Modified Cu/Diamond Interface. *J. Phys.: Condens. Matter* **2020**, *32*, 225001.
(26) Wu, J.; Wang, X.; Wang, Q.; Lou, Z.; Li, S.; Zhu, Y.; Qin, L.; Wei, H. Nanomaterials with Enzyme-Like Characteristics (Nanozymes): Next-Generation Artificial Enzymes (II). *Chem. Soc. Rev.* **2019**, *48*, 1004−1076.
(27) Liang, M.; Yan, X. Nanozymes: from New Concepts, Mechanisms, and Standards to Applications. *Acc. Chem. Res.* **2019**, *52*, 2190−2200.
(28) Gao, L.; Zhuang, J.; Nie, L.; Zhang, J.; Zhang, Y.; Gu, N.; Wang, T.; Feng, J.; Yang, D.; Perrett, S.; Yan, X. Intrinsic Peroxidase-Like Activity of Ferromagnetic Nanoparticles. *Nat. Nanotechnol.* **2007**, *2*, 577−583.
(29) Lu, N.; Zhang, M.; Ding, L.; Zheng, J.; Zeng, C.; Wen, Y.; Liu, G.; Aldalbahi, A.; Shi, J.; Song, S.; et al. Yolk-Shell Nanostructured Fe_3O_4@C Magnetic Nanoparticles with Enhanced Peroxidase-Like Activity for Label-Free Colorimetric Detection of H_2O_2 and Glucose. *Nanoscale* **2017**, *9*, 4508−4515.
(30) Shutov, R. V.; Guerreiro, A.; Moczko, E.; de Vargas-Sansalvador, I. P.; Chianella, I.; Whitcombe, M. J.; Piletsky, S. A. Introducing MINA-the Molecularly Imprinted Nanoparticle Assay. *Small* **2014**, *10*, 1086−1089.
(31) Wu, Y.-S.; Huang, F.-F.; Lin, Y.-W. Fluorescent Detection of Lead in Environmental Water and Urine Samples Using Enzyme Mimics of Catechin-Synthesized Au Nanoparticles. *ACS Appl. Mater. Interfaces* **2013**, *5*, 1503−1509.
(32) Kim, M.; Kim, M. S.; Kweon, S. H.; Jeong, S.; Kang, M. H.; Kim, M. I.; Lee, J.; Doh, J. Simple and Sensitive Point-of-Care Bioassay System Based on Hierarchically Structured Enzyme-Mimetic Nanoparticles. *Adv. Healthcare Mater.* **2015**, *4*, 1311−1316.
(33) Samuel, E. L. G.; Marcano, D. C.; Berka, V.; Bitner, B. R.; Wu, G.; Potter, A.; Fabian, R. H.; Pautler, R. G.; Kent, T. A.; Tsai, A.-L.; Tour, J. M. Highly Efficient Conversion of Superoxide to Oxygen Using Hydrophilic Carbon Clusters. *Proc. Natl. Acad. Sci. U. S. A.* **2015**, *112*, 2343−2348.
(34) Zhang, J.; Lu, N.; Peng, H.; Li, J.; Yan, R.; Shi, X.; Ma, P.; Lv, M.; Wang, L.; Tang, Z.; Zhang, M. Multi-Triggered and Enzyme-Mimicking Graphene Oxide/Polyvinyl Alcohol/G-Quartet Supramolecular Hydrogels. *Nanoscale* **2020**, *12*, 5186−5195.
(35) Nath, I.; Chakraborty, J.; Verpoort, F. Metal Organic Frameworks Mimicking Natural Enzymes: A Structural and Functional Analogy. *Chem. Soc. Rev.* **2016**, *45*, 4127−4170.
(36) Plonka, A. M.; Wang, Q.; Gordon, W. O.; Balboa, A.; Troya, D.; Guo, W.; Sharp, C. H.; Senanayake, S. D.; Morris, J. R.; Hill, C. L.; Frenkel, A. I. In Situ Probes of Capture and Decomposition of

https://doi.org/10.1021/acsami.1c04241
ACS Appl. Mater. Interfaces 2021, 13, 21040−21050

Chemical Warfare Agent Simulants by Zr-Based Metal Organic Frameworks. *J. Am. Chem. Soc.* **2017**, *139*, 599−602.
(37) Wu, J.; Wang, Z.; Jin, X.; Zhang, S.; Li, T.; Zhang, Y.; Xing, H.; Yu, Y.; Zhang, H.; Gao, X.; Wei, H. Hammett Relationship in Oxidase-Mimicking Metal-Organic Frameworks Revealed Through a Protein-Engineering-Inspired Strategy. *Adv. Mater.* **2021**, *33*, 2005024.
(38) Duan, D.; Fan, K.; Zhang, D.; Tan, S.; Liang, M.; Liu, Y.; Zhang, J.; Zhang, P.; Liu, W.; Qiu, X.; et al. Nanozyme-Strip for Rapid Local Diagnosis of Ebola. *Biosens. Bioelectron.* **2015**, *74*, 134−141.
(39) Farka, Z. k.; Čunderlová, V.; Horáčková, V.; Pastucha, M. j.; Mikušová, Z.; Hlaváček, A. n.; Skládal, P. Prussian Blue Nanoparticles as A Catalytic Label in A Sandwich Nanozyme-Linked Immunosorbent Assay. *Anal. Chem.* **2018**, *90*, 2348−2354.
(40) Zhang, R.; Lu, N.; Zhang, J.; Yan, R.; Li, J.; Wang, L.; Wang, N.; Lv, M.; Zhang, M. Ultrasensitive Aptamer-Based Protein Assays Based on One-Dimensional Core-Shell Nanozymes. *Biosens. Bioelectron.* **2020**, *150*, 111881.
(41) Wu, J.; Lv, W.; Yang, Q.; Li, H.; Li, F. Label-Free Homogeneous Electrochemical Detection of MicroRNA Based on Target-Induced Anti-Shielding Against the Catalytic Activity of Two-Dimension Nanozyme. *Biosens. Bioelectron.* **2021**, *171*, 112707.
(42) Fan, K.; Xi, J.; Fan, L.; Wang, P.; Zhu, C.; Tang, Y.; Xu, X.; Liang, M.; Jiang, B.; Yan, X.; Gao, L. In Vivo Guiding Nitrogen-Doped Carbon Nanozyme for Tumor Catalytic Therapy. *Nat. Commun.* **2018**, *9*, 1440.
(43) Zhu, Y.; Wang, W.; Cheng, J.; Qu, Y.; Dai, Y.; Liu, M.; Yu, J.; Wang, C.; Wang, H.; Wang, S.; et al. Stimuli-Responsive Manganese Single-Atom Nanozyme for Tumor Therapy via Integrated Cascade Reactions. *Angew. Chem.* **2021**, *133*, 9566−9574.
(44) Liu, Y.; Wang, J.; Xiong, Q.; Hornburg, D.; Tao, W.; Farokhzad, O. C. Nano-Bio Interactions in Cancer: From Therapeutics Delivery to Early Detection. *Acc. Chem. Res.* **2021**, *54*, 291−301.
(45) Liu, M.; Zhao, H.; Chen, S.; Yu, H.; Quan, X. Interface Engineering Catalytic Graphene for Smart Colorimetric Biosensing. *ACS Nano* **2012**, *6*, 3142−3151.
(46) Zeng, C.; Lu, N.; Wen, Y.; Liu, G.; Zhang, R.; Zhang, J.; Wang, F.; Liu, X.; Li, Q.; Tang, Z.; Zhang, M. Engineering Nanozymes Using DNA for Catalytic Regulation. *ACS Appl. Mater. Interfaces* **2019**, *11*, 1790−1799.
(47) Liu, B.; Liu, J. Accelerating Peroxidase Mimicking Nanozymes Using DNA. *Nanoscale* **2015**, *7*, 13831−13835.
(48) Zhang, L.; Qi, Z.; Zou, Y.; Zhang, J.; Xia, W.; Zhang, R.; He, Z.; Cai, X.; Lin, Y.; Duan, S.-Z.; et al. Engineering DNA-Nanozyme Interfaces for Rapid Detection of Dental Bacteria. *ACS Appl. Mater. Interfaces* **2019**, *11*, 30640−30647.
(49) Masud, M. K.; Na, J.; Younus, M.; Hossain, M. S. A.; Bando, Y.; Shiddiky, M. J.; Yamauchi, Y. Superparamagnetic Nanoarchitectures for Disease-Specific Biomarker Detection. *Chem. Soc. Rev.* **2019**, *48*, 5717−5751.
(50) Song, Y.; Qu, K.; Zhao, C.; Ren, J.; Qu, X. Graphene Oxide: Intrinsic Peroxidase Catalytic Activity and Its Application to Glucose Detection. *Adv. Mater.* **2010**, *22*, 2206−2210.
(51) Kim, E.; Lee, S. G.; Kim, H.-C.; Lee, S. J.; Baek, C. S.; Jeong, S. W. Protein-Directed Immobilization of Phosphocholine Ligands on A Gold Surface for Multivalent C-Reactive Protein Binding. *Curr. Top. Med. Chem.* **2013**, *13*, 519−524.
(52) Li, P.; Deng, S.; Xu, Z. Z. Toxicant Substitutes In Immunological Assays for Mycotoxins Detection: A Mini Review. *Food Chem.* **2021**, *344*, 128589.
(53) Wang, C.; Du, X.; Xie, T.; Li, H. Label- and Modification-Free-Based In Situ Selection of Bovine Serum Albumin Specific Aptamer. *J. Sep. Sci.* **2019**, *42*, 3571−3578.
(54) Deng, R.; Xie, X.; Vendrell, M.; Chang, Y.-T.; Liu, X. Intracellular Glutathione Detection Using MnO_2-Nanosheet-Modified Upconversion Nanoparticles. *J. Am. Chem. Soc.* **2011**, *133*, 20168−20171.
(55) Umezawa, K.; Yoshida, M.; Kamiya, M.; Yamasoba, T.; Urano, Y. Rational Design of Reversible Fluorescent Probes for Live-Cell Imaging and Quantification of Fast Glutathione Dynamics. *Nat. Chem.* **2017**, *9*, 279−286.
(56) Yu, F.; Huang, Y.; Cole, A. J.; Yang, V. C. The Artificial Peroxidase Activity of Magnetic Iron Oxide Nanoparticles and Its Application to Glucose Detection. *Biomaterials* **2009**, *30*, 4716−4722.

https://doi.org/10.1021/acsami.1c04241
ACS Appl. Mater. Interfaces 2021, 13, 21040−21050